JACS
JOURNAL OF THE AMERICAN CHEMICAL SOCIETY

Article

pubs.acs.org/JACS

Photofunctional Construct That Interfaces Molecular Cobalt-Based Catalysts for H_2 Production to a Visible-Light-Absorbing Semiconductor

Alexandra Krawicz, Jinhui Yang, Eitan Anzenberg, Junko Yano,* Ian D. Sharp,* and Gary F. Moore*

Joint Center for Artificial Photosynthesis (JCAP), Lawrence Berkeley National Laboratory, Berkeley, California 94720, United States

Supporting Information

ABSTRACT: Molecular cobalt-containing hydrogen production catalysts are grafted to a visible-light-absorbing semiconductor. The attachment procedure exploits the UV-induced immobilization chemistry of vinylpyridine to p-type (100) gallium phosphide (GaP). Single step surface-initiated photopolymerization yields a covalently attached polymer with pendent pyridyl groups that provide attachment points for assembling cobaloxime catalysts. Successful attachment is characterized by grazing angle attenuated total reflection Fourier transform infrared spectroscopy (GATR-FTIR), which shows distinct vibrational modes associated with the catalyst, as well as X-ray photoelectron spectroscopy (XPS) and X-ray absorption near edge structure spectroscopy (XANES) that confirm the presence of intact Co^{III} complex on the surface. The Co-functionalized photocathode shows significantly enhanced photoelectrochemical (PEC) performance in aqueous conditions at neutral pH, compared to results obtained on GaP without attached cobalt complex. PEC measurements, at 100 mW cm^{-2} illumination, yield a 2.4 mA cm^{-2} current density at a 310 mV underpotential.

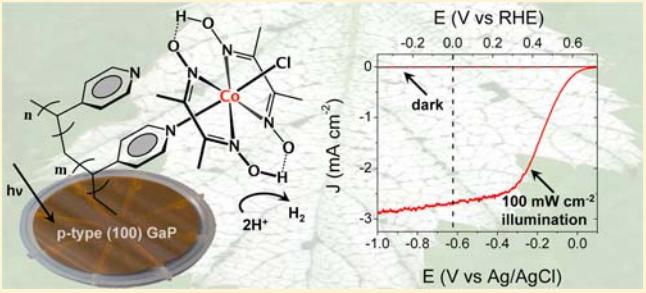

INTRODUCTION

Artificial photosynthesis has been described as a great scientific and moral challenge of our time.[1] It offers a promising approach to meeting global human energy demands with minimal environmental impact.[2] Yet many scientific and engineering challenges must be addressed for its realization.[3] Among these are development of effective strategies for interfacing newly emerging energy transduction catalysts and light absorbers. In this context, the development of advanced materials and techniques for manipulating matter on the nanoscale has allowed significant advancements including attachment of molecular sensitizers and catalysts to wide band gap semiconductors for developing integrated photoanodes and photocathodes.[4] Recently, we reported a modular approach to interfacing molecular catalysts to visible-light-absorbing semiconductors including p-type (100) GaP (E_g = 2.26 eV) and p-type (111) Si (E_g = 1.12 eV).[5] Both materials have conduction bands poised negative of the H^+/H_2 redox couple and are thus relevant for light capture and conversion applications in artificial photosynthesis.[6]

Herein we report a photochemically active construct composed of molecular cobalt-containing hydrogen production catalysts attached to GaP. The catalysts belong to the cobaloxime class of compounds that have shown recent promise in electrocatalysis and solar-to-fuels applications.[7] By use of a two-step method (Scheme 1), vinylpyridine is first photochemically grafted to the (100) GaP surface and then catalyst attachment is achieved by chemical treatment of the polyvinylpyridine (PVP) functionalized surface with a solution containing the cobaloxime catalyst precursor $Co(dmgH_2)(dmgH)Cl_2$[8,9] (see Methods for details). Verification of synthetic efforts is achieved using surface sensitive spectroscopic methods including grazing angle attenuated total reflection spectroscopy (GATR-FTIR), X-ray photoelectron spectroscopy (XPS), and X-ray absorption near edge structure spectroscopy (XANES), providing evidence for formation of surface-grafted polymers[10] containing pyridine units with attached cobaloxime complexes.

Although the concepts of artificial photosynthesis and improvement of photochemical fuel generation by surface modification of semiconductor photocathodes are not new,[11] examples of photofunctional systems composed of molecular catalysts attached to visible-light-absorbing semiconductors are critically lacking. This work represents a promising step toward developing an integrated photocathode material for use in a tandem solar-fuels generator and is a significant advancement from previous work on attaching similar catalysts to UV-absorbing (TiO_2) or nonphotoactive (carbon and conductive metal oxide) substrates. Further, using a polymeric linker for surface functionalization allows use of a broad range of vinyl monomers with a variety of functional groups, giving additional control over surface loading capacity and attachment stability of catalysts as new materials and discoveries emerge.

Received: April 26, 2013
Published: July 12, 2013

   dx.doi.org/10.1021/ja404158r | J. Am. Chem. Soc. 2013, 135, 11861−11868

Scheme 1. Schematic Representation of the Attachment Method Used To Assemble Modified Photocathodes

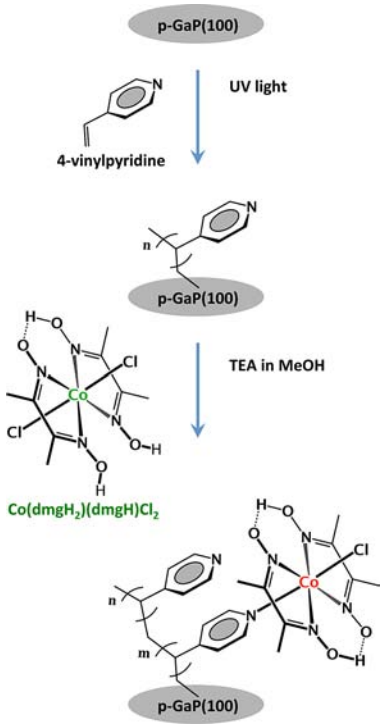

RESULTS AND DISCUSSION

Sample preparation starts with buffered hydrofluoric acid etching of GaP to remove the surface oxide film and provide hydroxyl-terminated surface sites for UV-initiated photochemical attachment of linker molecules.[5] Polymer growth is achieved by reacting 4-vinylpyridine with the hydroxylated surface. It is postulated that this reaction takes place via the self-initiated photografting and photopolymerization (SIPGP) mechanism,[12] which has been reported on a variety of hydrogen- and hydroxyl-terminated materials[13] and occurs when hydrogen is abstracted from the surface by a photoactivated monomer to begin surface-initiated free radical polymerization. This approach provides polymers bearing multiple pyridine binding sites per chain, thereby significantly increasing the per geometric area loading capacity of catalysts on the semiconductor compared to approaches using self-assembled monolayers of molecular linkers. GATR-FTIR, XPS, and XANES provide converging evidence that catalyst attachment occurs by replacement of one of the axial chloride ligands of $Co(dmgH_2)(dmgH)Cl_2$ with a surface attached pyridine moiety. Charge balance for replacing chloride, an anionic X-type ligand, with pyridyl, a neutral L-type ligand, is accounted for by the base promoted conversion of the dimethylglyoxime ligand to the dimethylglyoximate monoanion (Scheme 1).

GATR-FTIR spectra of (100) GaP, including spectra collected following photochemical grafting of vinylpyridine and after treatment with the cobalt catalyst precursor, are shown in Figure 1. A FTIR spectrum of 4-vinylpyridine in KBr and a FTIR spectrum of the cobaloxime catalyst, $Co(dmgH)_2PyCl$,[9] in KBr are shown for comparison. The frequencies of the five absorption bands centered in the 1400−1600 cm^{-1} range on PVP-functionalized GaP surfaces confirm the formation of a polymer graft with the planar

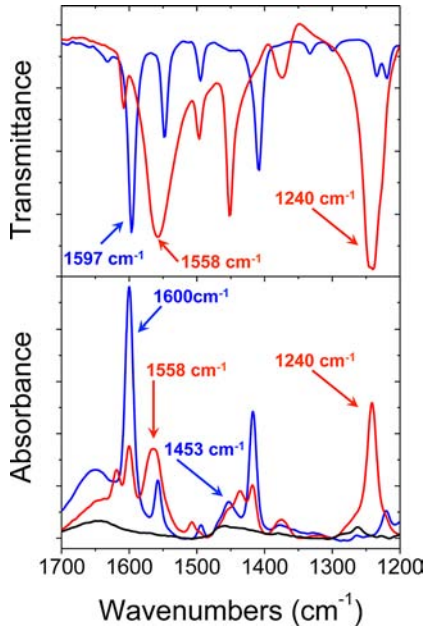

Figure 1. (Top) FTIR transmission spectra of 4-vinylpyrdine in KBr (blue) and the cobaloxime catalyst $Co(dmgH)_2PyCl$ in KBr (red). (Bottom) GATR-FTIR spectra of GaP following buffered HF treatment (black), polyvinylpyridine-grafted GaP (blue), and cobaloxime-modified GaP (red).

deformation vibration of the CH_2 groups in the polymer chain contributing to the mode at 1453 cm^{-1}.[14] Indeed, this mode is not observed in 4-vinylpyridine but is present in polymeric materials such as polystyrene, poly(2-vinylpyridine), and poly(4-vinylpyridine). Following treatment of the PVP-grafted surface with $Co(dmgH_2)(dmgH)Cl_2$, vibrational modes characteristic of $Co(dmgH)_2PyCl$, including distinct absorption bands associated with pyridine units attached to cobaloxime complexes and a strong NO^- stretching frequency at 1240 cm^{-1}, are observed on the functionalized surface. In $Co(dmgH_2)(dmgH)Cl_2$, the precursor material used to assemble the attached cobalt complex to the PVP-functionalized electrode, the NO^- vibration is centered at 1225 cm^{-1} (Figure 2). The uncoordinated dimethylglyoxime has no band in this region.

The presence of intact Co complex is further confirmed by XPS. Survey spectra of cobaloxime-modified GaP show the presence of C, N, O, Cl, and Co elements of the catalyst

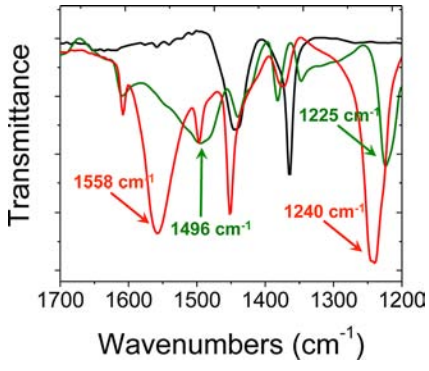

Figure 2. FTIR transmission spectra of $Co(dmgH)_2PyCl$ in KBr (red), $Co(dmgH_2)(dmgH)Cl_2$ in KBr (green), and dimethlgyloxime ($dmgH_2$) in KBr (black).

dx.doi.org/10.1021/ja404158r | J. Am. Chem. Soc. 2013, 135, 11861−11868

(Figure S5). N 1s core level spectra of GaP samples following photochemical grafting of vinylpyridine show a single feature centered at 398.7 eV (Figure 3a). However, following catalyst

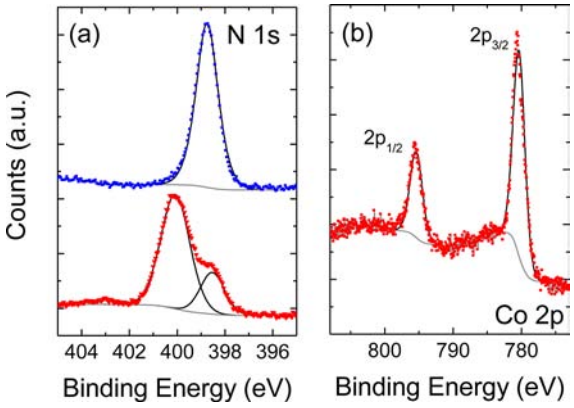

Figure 3. (a) N 1s core level XPS spectra of polyvinylpyridine-grafted GaP (blue) and cobaloxime-modified GaP (red). (b) Co 2p core level XPS spectra of cobaloxime-modified GaP. The solid gray line is the Shirley background, and the solid black lines are the component fits.

immobilization, a second N 1s spectral contribution, centered at 400.1 eV, is observed. Comparison with core level N 1s spectra of a $Co(dmgH)_2PyCl$ powder sample (Figure S6) indicates that the 400.1 eV peak includes contributions from the glyoximate ligand, as well as Co-coordinated pyridine. The remnant contribution at lower binding energies is assigned to pyridine units on the polymer that are not coordinated to Co. In addition, Co 2p core level spectra of cobaloxime-modified GaP (Figure 3b) show peaks centered at 780.5 eV ($2p_{3/2}$) and 795.5 eV ($2p_{1/2}$), with the expected 2:1 branching ratio. The 15.0 eV peak separation and lack of pronounced shakeup satellite features are characteristic of the Co^{III} oxidation state[15] and are consistent with previous reports of similar, yet structurally different, cobaloxime catalysts attached to carbon nanotubes (CNTs)[7b] or mesoporous metal oxide.[7c] Analysis of the relative intensities of the Cl 2p and Co 2p core level spectra provides additional evidence that molecular assembly occurs by replacement of one axial chloride ligand of $Co(dmgH_2)(dmgH)Cl_2$ with a pyridyl group. The measured Co/Cl ratio of a $Co(dmgH_2)(dmgH)Cl_2$ powder sample is 1:1.9. However, for cobaloxime-modified GaP the measured Co/Cl ratio is 1:1.1, consistent with the proposed reaction scheme.

Co K-edge XANES spectra provide additional evidence for successful attachment of intact Co catalyst. As shown in Figure 4, the XANES spectrum of the precursor material used to assemble the attached cobalt complex to the PVP-functionalized electrode, $Co(dmgH_2)(dmgH)Cl_2$, is characterized by an edge feature at 7723 eV. However, this feature is not pronounced in the spectrum of $Co(dmgH)_2PyCl$ or in spectra of cobaloxime-modified electrodes. Furthermore, as shown in the lower panel of Figure 4, the XANES spectrum of the model $Co(dmgH)_2PyCl$ is nearly identical to the grazing incidence XANES spectrum of the cobaloxime-modified electrode, indicating that surface immobilized catalysts have a geometrical symmetry and electronic structure that is similar to that of the unbound $Co(dmgH)_2PyCl$ complex.

Spectroscopic ellipsometry measurements were performed in air and yielded a PVP thickness of ~12 nm following the grafting procedure (see Methods and Supporting Information for details). The thickness of the solvent-free brush layer

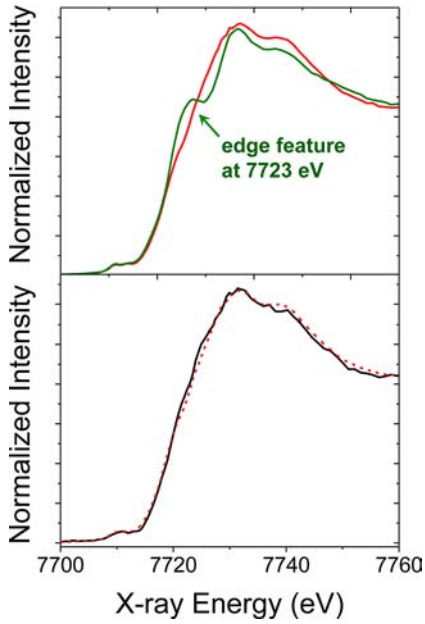

Figure 4. (Top) Co K-edge XANES spectra of $Co(dmgH)_2PyCl$ (red) and $Co(dmgH_2)(dmgH)Cl_2$ (green). (Bottom) Cobaloxime-modified GaP (black) compared to $Co(dmgH)_2PyCl$ (red dash) (shown in upper panel as red solid line).

provides an estimate of the pyridyl site density on the surface, since the bulk PVP density (1.15 g cm^{-3}) is representative of the solvent-free layer density. However, if solvent remains following cleaning and drying, then the calculated value provides an upper limit on the site density. For the present case, with a 12 nm thick dry PVP layer, the maximum site density is 7.9×10^{15} cm^{-2} = 13 nmol cm^{-2}.

The Co-functionalized photocathode shows significantly enhanced photoelectrochemical (PEC) performance in aqueous solutions buffered at pH 7 (1 M phosphate buffer) and in unbuffered conditions (0.1 M Na_2SO_4), compared to unfunctionalized or PVP-grafted GaP (Figure 5 and Figure S9). PEC testing, at 100 mW cm^{-2} illumination using a Newport Oriel Apex illuminator source, yields a 2.4 mA cm^{-2} current density when operating at a potential 310 mV below the equilibrium potential of the H^+/H_2 redox couple. To

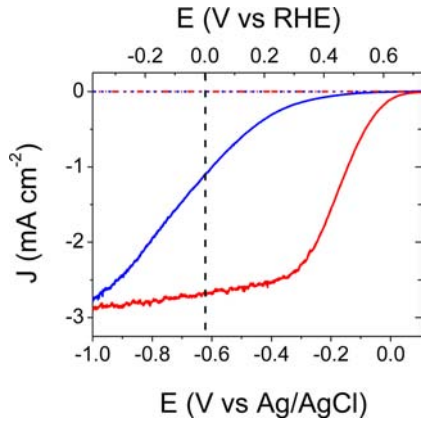

Figure 5. Linear sweep voltammograms of polyvinylpyridine-grafted GaP (blue) and cobaloxime-modified GaP (red) working electrodes at pH 7 in the dark (dashed lines) and with 100 mW cm^{-2} illumination (solid lines).

dx.doi.org/10.1021/ja404158r | J. Am. Chem. Soc. 2013, 135, 11861−11868

achieve a similar photocurrent density using electrodes without cobaloxime modification (i.e., the PVP-grafted GaP cathode), a 270 mV overpotential must be applied. For comparison, a previously reported cobaloxime-modified CNTs electrocatalyst[7b] requires a 590 mV overpotential to reach a current density of 1 mA cm^{-2}. Of course in this case the current densities are not dependent on illumination of the sample.

The open circuit photovoltage for the PVP-grafted and cobaloxime-modified GaP electrodes Figure 5 are +0.69 and +0.76 V vs RHE, respectively. The positive shift in open circuit photovoltage following modification of the PVP-modified GaP electrode with cobaloximes is indicative of the increased photoactivity of these electrodes. In addition to the positive shift of the open circuit voltage, the fill factor for the *JV* response under illumination improves dramatically with incorporation of the Co catalyst (a >200% increase). For the PVP-grafted surface (without catalyst), the lack of active catalytic sites results in a greater probability for minority carrier recombination at the interface. Therefore, a more negative applied potential, which increases the surface band bending and suppresses charge carrier recombination, is required to achieve a given photocurrent density. For cobaloxime-modified samples, the incorporation of active Co catalysts promotes charge transfer across the interface.

Three-electrode electrolysis performed at +0.17 V vs RHE with illumination from a Solar Light PV cell test simulator at 100 mW cm^{-2} shows that the current produced with the cobaloxime-modified cathode is relatively stable, with only a 17% reduction in photocurrent after 5 min of irradiation (Figure 6). Experiments using an unfunctionalized (buffered HF treated) GaP electrode under the same conditions show a 76% reduction in photocurrent. In all examples a significant fraction of the photocurrent reduction (~10% in the case of the cobaloxime-modified electrode) is due to an initial capacitance spike, which is not a consequence of physical degradation. In addition, hydrogen bubbles, accumulating on the cobaloxime-modified photocathode surface during PEC operation, inhibit diffusion of electrolyte to the photocathode and contribute to the diminution of photocurrent.

The overall lower current densities observed in the controlled potential electrolysis measurements, compared to those observed in the linear sweep voltammetry measurements, are in part attributed to the spectral mismatch of the different lamps used in these experiments. All electrolysis measurements were performed on samples following identical linear sweep voltammetry dark/light testing of the individual samples. These results show that the *JV* response of the electrodes depends on the illumination conditions (i.e., the spectral profile of the Newport Oriel Apex illuminator is better matched to the absorption profile of GaP, allowing achievement of relatively higher photocurrent densities). The Solar Light PV cell test simulator offers illumination conditions that are more similar to AM1.5 solar illumination. However, results obtained using the Newport Oriel Apex illuminator indicate that photocarrier transport to the interface, rather than catalytic activity, limits the performance of the Co-modified GaP photocathodes at simulated AM1.5 illumination. This suggests that additional performance gains may be obtained by using semiconductors with improved absorption properties that are better matched to the solar spectrum and thus capable of achieving higher photocurrent densities. We conclude that polymer grafting alleviates the unstable photocurrent associated with the bare GaP surface, likely by providing a protective polymeric layer

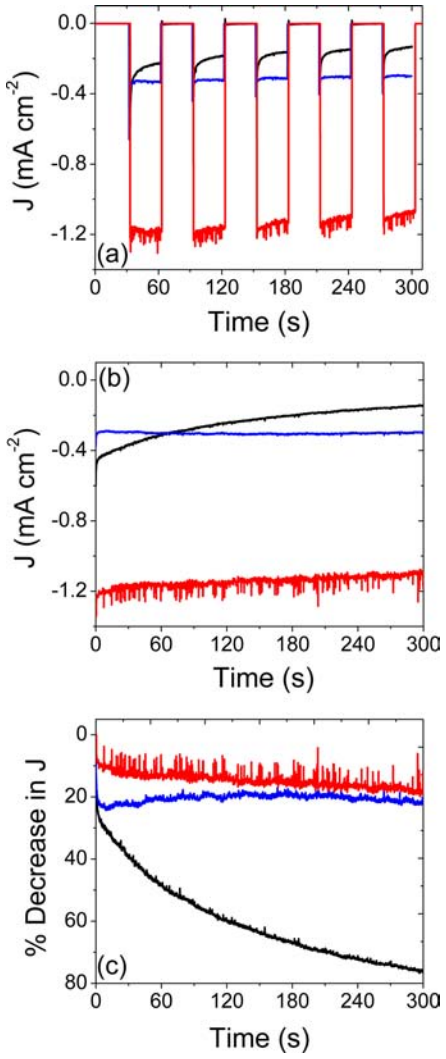

Figure 6. Three-electrode electrolysis measurements using GaP working electrodes following BHF treatment (black), polyvinylpyridine grafting (blue), and cobaloxime attachment (red), including data collected with (a) chopped (light on/light off) and (b, c) continuous simulated solar illumination. All measurements were performed at +0.17 V vs RHE.

that inhibits access to reactive surface sites. Functionalizing the pendent pyridyl groups of the surface attached polymer with cobaloxime catalysts provides additional improvement in photoperformance by lowering the potential requirements for achieving a given current density. Although the modified electrodes exhibit extended stability relative to unfunctionalized GaP, the photocurrent declines with time.

To investigate the origin of this performance reduction, surface analysis was performed following PEC operation. Both XPS (Figure 7) and XANES (Figure 8) measurements confirm the presence of intact cobalt complex on the surface following photoelectrochemical testing. While a reduction of the Co 2p core level intensity is observed, the XPS spectrum shows features characteristic of the prephotoelectrolysis state including two peaks associated with the $2p_{3/2}$ and $2p_{1/2}$ core levels of the cobaloxime complex separated by 15.0 eV, a lack of pronounced shakeup satellite features, and no observable features characteristic of cobaloxime decomposition products. Likewise, grazing angle XANES spectra show that the cobalt K-edges of surface grafted complexes, both prior to and following

dx.doi.org/10.1021/ja404158r | J. Am. Chem. Soc. 2013, 135, 11861−11868

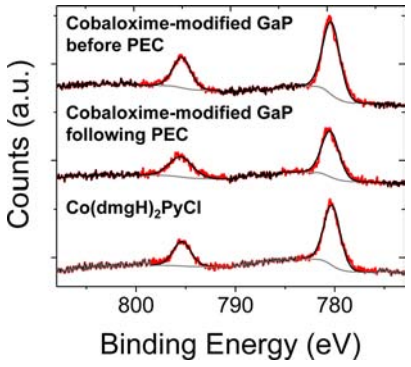

Figure 7. Co 2p core level XPS spectra of (top) cobaloxime-modified GaP prior to photoelectrochemical testing and (middle) following testing and (bottom) a reference sample of $Co(dmgH)_2PyCl$ powder. The solid gray lines are the Shirley background, and the solid black lines are the component fits.

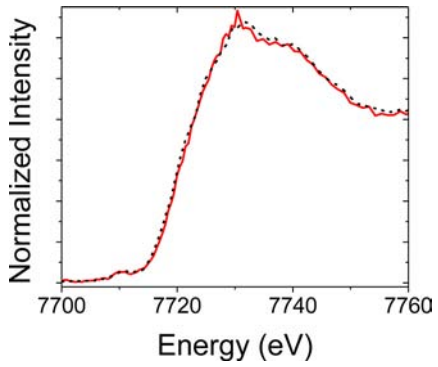

Figure 8. Co K-edge XANES spectra of cobaloxime-modified GaP following photoelectrochemical testing (red) and, for comparison, prior to photoelectrochemical testing (black dash) (shown in lower panel of Figure 4 as black solid line).

PEC testing, are nearly identical to that observed in the spectrum of $Co(dmgH)_2PyCl$, providing compelling evidence that attached complexes have an electronic structure similar to that of $Co(dmgH)_2PyCl$ and that the ligand symmetry is maintained following electrochemical testing.

Given the decrease of the Co 2p XPS intensity following PEC operation, loss of surface attached catalysts is likely a major contributing factor in the reduction of photocurrent with time. While a detailed analysis of all possible degradation pathways is currently unavailable, detachment of catalysts from surface grafted pyridines seems a likely point of failure; previous computational and experimental work indicates that the axial pyridine of similar cobaloxime complexes can become labile during redox cycling.[7a,j,k] However, in our study the polymeric support used to assemble the catalyst may provide additional durability by offering a protective encapsulating environment, trapping cobalt complexes at redox active sites with abundant pyridine units and favoring reformation of the complex over loss to bulk solution. As the molecular and nanoscale properties that favor charge transport efficiency are identified, the modular nature of this approach should allow for modification of the attachment strategy and anchoring functionalities in future work.

The ability to distinguish heterogeneous from homogeneous catalysis has received renewed attention as perceptions have blurred with advances in nanomaterials, clusters, metal nanoparticles, and bioinspired hybrid systems; yet such distinctions remain pertinent to understanding and improving catalytic design features.[16] Although proving a mechanism for a given reaction (heterogeneous, homogeneous, molecular, or other) may not be possible, one can rule out mechanisms that are inconsistent with available data. Our present data, complicated by heterogeneity,[17] are insufficient to resolve a detailed operating mechanism but are consistent with molecular catalysis (i.e., surface analysis following PEC testing of cobaloxime-modified electrodes indicates attached catalysts remain intact).

■ CONCLUSIONS

Surface sensitive spectroscopic methods verify our synthetic efforts dedicated to construction of a hybrid composite material that structurally interfaces a cobalt-containing hydrogen evolution catalyst to a visible-light-absorbing semiconductor. The modular-assembly method allows use of a broad range of functional vinyl monomers, giving additional control over the attachment and surface loading capacity of catalysts as new materials and discoveries emerge. Thus, the construct sets the stage for a better understanding of the relationship between catalyst placement, band edge energetics, and the resulting surface potential profile at the interface. In addition, multifunctional polymers, generated via copolymerization strategies, can be envisioned as scaffolds for tandem[18] catalytic systems, a promising feature in the context of CO_2 reduction. The cobaloxime-functionalized photocathode described here shows significantly enhanced photochemical performance in aqueous conditions at neutral pH, compared to results obtained on GaP without attached cobalt complex. Production of a 2.4 mA cm^{-2} current density at a 310 mV underpotential, indicates only light and no external electrochemical forward biasing or sacrificial electron donors, is required to generate the photocurrent.

■ METHODS

Materials and Synthesis. Single crystalline (100) GaP wafers were purchased from University Wafer. The wafers were p-type doped with Zn, yielding a resistivity of 1.17×10^{-1} Ω·cm, a mobility of 77 $cm^2\ V^{-1}\ s^{-1}$, and a carrier concentration of 6.95×10^{17} cm^{-3}. Extended defects result in an etch pit density (EPD) of 4.5×10^4 cm^{-2}. The material was single side polished to an epi-ready finish. Diced semiconductor samples were degreased by wiping the surface with an acetone soaked cotton swab and sonication in acetone and isopropanol for 5 min each, followed by drying under flowing nitrogen. Samples were then exposed to an air-generated oxygen plasma (Harrick Plasma, U.S.) at 30 W for 2 min. Surface oxide layers were then removed in a glovebox by immersion of the plasma-treated samples in buffered hydrofluoric acid (6:1 HF/NH_4F in H_2O) for 5 min, followed by rinsing with anhydrous methanol and drying under vacuum.

All syntheses were carried out under an argon atmosphere using Schlenk techniques or in a nitrogen glovebox. All reagents were purchased from Aldrich. All solvents were stored over the appropriate molecular sieves prior to use. Milli-Q water (18.2 MΩ·cm) was used to prepare all aqueous solutions. The cobaloxime catalyst precursor, $Co(dmgH_2)(dmgH)Cl_2$, and the cobaloxime catalyst, $Co(dmgH)_2PyCl$, were prepared according to a previously reported procedure.[9]

Preparation of Polyvinylpyridine-Grafted GaP. Freshly cleaned and etched (100) GaP wafers were placed in a quartz flask and covered with inhibitor-free 4-vinylpyridine. The flask was illuminated with UV light (254 nm, Spectroliner E-series UV lamp) for 2 h with the polished surface of GaP facing the light source. The modified wafers were then sonicated and washed with anhydrous methanol before drying under vacuum.

Preparation of Cobaloxime-Modified GaP. PVP-grafted wafers of (100) GaP were dipped in a solution of $Co(dmgH_2)(dmgH)Cl_2$ (1

dx.doi.org/10.1021/ja404158r | J. Am. Chem. Soc. 2013, 135, 11861−11868

mM in methanol) in the presence of triethylamine (1 mM in methanol) overnight. The modified wafers were rinsed with methanol and isopropanol before drying under nitrogen.

Preparation of Electrodes. GaP working electrodes were fabricated by applying an indium−gallium eutectic (Aldrich) to the backside of a wafer, then fixing a copper wire to the back of the wafer using a conductive silver epoxy (Circuit Works). The copper wire was passed through a glass tube, and the wafer was insulated and attached to the glass tube with Loctite 615 Hysol Epoxi-patch adhesive. The epoxy was allowed to dry overnight before testing the electrodes.

Instrument Descriptions and Experimental Details. *UV–Visible.* Ultraviolet−visible (UV−vis) optical spectra were recorded on a Shimadzu SolidSpec-3700 spectrometer with a D_2 (deuterium) lamp for the ultraviolet range and a WI (halogen) lamp for the visible and near-infrared. Transmission and reflectance measurements were performed with an integrating sphere.

NMR. Nuclear magnetic resonance (NMR) spectra were recorded on a Bruker 500′54 Ascend spectrometer operating at 500 MHz. Unless otherwise stated, all spectra were collected at room temperature.

FTIR. Grazing angle attenuated total reflection Fourier transform infrared spectroscopy (GATR-FTIR) was performed using a VariGATR accessory (Harrick Scientific) with a Ge crystal plate installed in a Bruker Vertex 70. Samples were pressed against the Ge crystal to ensure effective optical coupling. Spectra were collected under a dry nitrogen purge with a 4 cm^{-1} resolution, GloBar MIR source, a broadband KBr beamsplitter, and a liquid nitrogen cooled MCT detector. Background measurements were obtained from the bare Ge crystal. Spectra from model compounds in pressed KBr pellets were acquired with the same settings in transmission mode.

XPS. X-ray photoelectron spectroscopy (XPS) was performed using a monochromatized Al Kα source ($h\nu$ = 1486.6 eV), operated at 225 W, on a Kratos Axis Ultra DLD system at a takeoff angle of 0° relative to the surface normal and a pass energy for narrow scan spectra of 20 eV, corresponding to an instrument resolution of approximately 600 meV. Survey spectra were collected with a pass energy of 80 eV. Spectral fitting was performed using Casa XPS analysis software. Spectral positions were corrected by shifting the primary C 1s core level position to 284.8 eV, and curves were fit with quasi-Voigt lines following Shirley background subtraction. For post-PEC XPS analysis, electrochemical testing was performed on a sample following initial XPS measurements. Electrochemical testing consisted of five consecutive linear sweep voltammograms (in the range of +0.30 to −1.00 V vs Ag/AgCl at a scan rate of 100 mV s^{-1}) in 1 M phosphate buffer under a continuous flow of 5% hydrogen in nitrogen. The initial sweep was performed in the dark and the following under 100 mW cm^{-2}. The sample was rinsed with Milli-Q water and dried before XPS measurements.

Co K-Edge XANES. Data from X-ray absorption near edge structure spectroscopy (XANES) were collected at the Advanced Light Source (ALS) on beamline 10.3.2 with an electron energy of 1.9 GeV and an average current of 500 mA. The radiation was monochromatized by a Si(111) double-crystal monochromator. The intensity of the incident X-ray was monitored by an N_2-filled ionization chamber (I_0) in front of the sample. The energy was calculated using a glitch in the I_0 relative to the absorption edge of a Co foil. All data were collected at room temperature. Data reduction of the XAS spectra was performed using custom software. Preedge and postedge contributions were subtracted from the XAS spectra, and the result was normalized with respect to the edge jump. For post-PEC XANES analysis, electrochemical testing was performed on a electrode that had undergone electrochemical testing consisting of four consecutive linear sweep voltammograms (in the range of +0.30 to −1.00 V vs Ag/AgCl at a scan rate of 100 mV s^{-1}) in a 1 M phosphate buffer under a continuous flow of 5% hydrogen in nitrogen. The initial sweep was performed in the dark and the following under 100 mW cm^{-2} illumination. The sample was rinsed with Milli-Q water and dried before XANES measurements. The spectrum of a freshly prepared cobaloxime-modified electrode, with no prior PEC testing, was also collected.

Ellipsometry. Film thickness was determined using a Woollam α-SE ellipsometer with a spectral range of 381−893 nm. All measurements were at a 70° incidence angle. The parameters and model used to determine the PVP film thickness are described in the Supporting Information.

Electrochemistry. Cyclic voltammetry was performed with a Biologic potentiostat using a glassy carbon (3 mm diameter) disk, a platinum counter electrode, and a silver wire pseudoreference electrode in a conventional three-electrode cell. Anhydrous acetonitrile (Aldrich) was used as the solvent for electrochemical measurements. The supporting electrolyte was 0.10 M tetrabutylammonium hexafluorophosphate. The solution was deoxygenated by bubbling with argon. The working electrode was cleaned between experiments by polishing with alumina (50 nm diameter) slurry, followed by solvent rinses. The potential of the pseudoreference electrode was determined using the ferrocenium/ferrocene redox couple as an internal standard (with $E_{1/2}$ taken as 0.40 V vs NHE). The voltammograms were recorded at sweep rates of 100 mV s^{-1}.

Linear sweep voltammetry and three-electrode electrolysis (chronoamperometry) were performed with a Biologic potentiostat using a platinum counter electrode, a Ag/AgCl, NaCl (3 M) reference electrode (0.21 V vs NHE), and GaP working electrodes (including GaP following buffered HF treatment, PVP-grafted GaP, and cobaloxime-modified GaP) in a modified cell containing a quartz window. The supporting electrolyte was 1 M phosphate buffer (pH 7) or 0.1 M Na_2SO_4 (pH 6.3). All measurements were performed under a continuous flow of 5% hydrogen in nitrogen. Photoelectrochemical (PEC) testing was performed using two types of lamps. Linear sweep voltammetry was performed using a Newport Oriel Apex Illuminator model 71228 light source at 100 mW cm^{-2} illumination. Electrolysis was performed using a Solar Light PV cell test simulator model 16S-300-005V4.0 xenon lamp with an AM1.5 filter and a XPS-300 power supply at 100 mW cm^{-2} illumination. All data were recorded following initial light/dark testing.

GC. Confirmation of hydrogen generation via gas chromatography (GC) was performed using an Agilent 490 Micro GC with a column temperature of 50 °C and argon as the carrier gas. Gas samples were syringe injected using 10 mL aliquots of headspace gas collected with a Hamilton syringe from a sealed PEC cell both prior to and following 30 min of three-electrode photoelectrolysis using a cobaloxime modified working electrode poised at +0.17 V vs RHE. Prior to the experiment the cell was purged for 30 min with argon before sealing. The retention time of hydrogen was confirmed using a known source of hydrogen obtained from a standard lecture bottle containing a hydrogen and argon mixture.

■ ASSOCIATED CONTENT

Ⓢ Supporting Information

Optical characterization of materials, NMR spectra, FTIR data, XPS data, PVP film thickness determination via ellipsometry, electrochemical and photoelectrochemical data, GC data, listing of complete references. This material is available free of charge via the Internet at http://pubs.acs.org.

■ AUTHOR INFORMATION

Corresponding Author

jyano@lbl.gov; idsharp@lbl.gov; gfmoore@lbl.gov

Notes

The authors declare no competing financial interest.

■ ACKNOWLEDGMENTS

This material is based upon work performed by the Joint Center for Artificial Photosynthesis, a DOE Energy Innovation Hub, supported through the Office of Science of the U.S. Department of Energy under Award Number DE-SC0004993. XANES experiments were performed at the Advanced Light Source (beamline 10.3.2), operated under Contract DE-AC02-

05CH11231. The authors thank Dr. Sirine Fakra and Dr. Matthew Marcus for assistance with experiments performed at Advanced Light Source (beamline 10.3.2), Prof. Rachel Seaglman and Dr. Miguel Modestino for use of the ellipsometer, and Dr. Frank Deubel, Mark Hettick, and Dr. Diana Cedeno for discussions. The authors also thank Dr. Heinz Frei. The TOC photo was taken by Brandi Eide.

REFERENCES

(1) (a) Faunce, T. A.; Lubitz, W.; Rutherford, A. W.; MacFarlane, D.; Moore, G. F.; Yang, P.; Nocera, D. G.; Moore, T. A.; Gregory, D. H.; Fukuzumi, S.; et al. *Energy Environ. Sci.* **2013**, *6*, 695−698. (b) *New Sciences for a Secure and Sustainable Energy Future*; U.S. Department of Energy: Washington, DC, December 2008. (c) *Directing Matter and Energy: Five Challenges for Science and the Imagination*; U.S. Department of Energy: Washington, DC, December 2007. (d) Armaroli, N.; Balzani, V. *Angew. Chem., Int. Ed.* **2007**, *46*, 52−66.

(2) (a) Lewis, N. S.; Nocera, D. G. *Proc. Natl. Acad. Sci. U.S.A.* **2006**, *103*, 15729−15735. (b) Hoffert, M. I.; Caldeira, K.; Jain, A. K.; Haites, E. F.; Harvey, L. D. D.; Potter, S. D.; Schlesinger, M. E.; Schneider, S. H.; Watts, R. G.; Wigley, T. M. L.; Wuebbles, D. J. *Nature* **1998**, *395*, 881−884.

(3) (a) Tran, P. D.; Wong, L. H.; Barber, J.; Loo, J. S. C. *Energy Environ. Sci.* **2012**, *5*, 5902−5918. (b) Swierk, J. R.; Mallouk, T. E. *Chem. Soc. Rev.* **2012**, *42*, 2357−2387. (c) Najafpour, M. M.; Shen, J.-R.; Barber, J.; Moore, G. F.; Govindjee. *Chem. World* **2012**, No. November, 43. (d) Moore, G. F.; Brudvig, G. W. *Annu. Rev. Condens. Matter Phys.* **2011**, *2*, 303−327. (e) Blankenship, R. E.; Tiede, D. M.; Barber, J.; Brudvig, G. W.; Fleming, G.; Ghirardi, M.; Gunner, M. R.; Junge, W.; Kramer, D. M.; Melis, A.; et al. *Science* **2011**, *332*, 805−809. (f) Hammarström, L.; Winkler, J. R.; Gray, H. B.; Styring, S. *Science* **2011**, *333*, 288. (g) Walter, M. G.; Warren, E. L.; Mckone, J. R.; Boettcher, S. W.; Mi, Q.; Santori, E. A.; Lewis, N. S. *Chem. Rev.* **2010**, *110*, 6446−6473.

(4) (a) Gardner, J. M.; Beyler, M.; Karnahl, M.; Tschierlei, S.; Ott, S.; Hammarström, L. *J. Am. Chem. Soc.* **2012**, *134*, 19322−19325. (b) Zhao, Y.; Swierk, J. R.; Megiatto, J. D.; Sherman, B. S.; Youngblood, W. J.; Qin, D.; Lentz, D. M.; Moore, A. L.; Moore, T. A.; Gust, D.; et al. *Proc. Natl. Acad. Sci. U.S.A.* **2012**, *109*, 15612−15616. (c) Song, W.; Glasson, C. R. K.; Luo, H.; Hanson, K.; Brennaman, M. K.; Concepcion, J. J.; Meyer, T. J. *J. Phys. Chem. Lett.* **2011**, *2*, 1808−1813. (d) Lakadamyali, F.; Reisner, E. *Chem. Commun.* **2011**, *47*, 1695−1697. (e) Moore, G. F.; Blakemore, J. D.; Milot, R. L.; Hull, J. F.; Song, H.-e.; Cai, L.; Schmuttenmaer, C. A.; Crabtree, R. H.; Brudvig, G. W. *Energy Environ. Sci.* **2011**, *4*, 2389−2392. (f) Li, G.; Sproviero, E. M.; McNamara, W. R.; Snoeberger, R. C., 3rd; Crabtree, R. H.; Brudvig, G. W.; Batista, V. S. *J. Phys. Chem. B* **2010**, *114*, 14214−14222. (g) Li, L.; Duan, L.; Xu, Y.; Gorlov, M.; Hagfeldt, A.; Sun, L. *Chem. Commun.* **2010**, *46*, 7307−7309. (h) Brimblecombe, R.; Koo, A.; Dismukes, G. C.; Swiegers, G. F.; Spiccia, L. *J. Am. Chem. Soc.* **2010**, *132*, 2892−2894. (i) Youngblood, W. J.; Lee, S.-H. A.; Kobayashi, Y.; Hernandez-Pagan, E. A.; Hoertz, P. G.; Moore, T. A.; Moore, A. L.; Gust, D.; Mallouk, T. E. *J. Am. Chem. Soc.* **2009**, *131*, 926−927.

(5) Moore, G. F.; Sharp, I. D. *J. Phys. Chem. Lett.* **2013**, *4*, 568−572.

(6) (a) Sun, Y.; Sun, J.; Long, J.; Yang, P.; Chang, C. *Chem. Sci.* **2013**, *4*, 118−124. (b) Reece, S. Y.; Hamel, J. A.; Sung, K.; Jarvi, T. D.; Esswein, A. J.; Pijpers, J. J. H.; Nocera, D. G. *Science* **2012**, *334*, 645−648. (c) Kaiser, B.; Fertig, D.; Ziegler, J.; Klett, J.; Hoch, S.; Jaegermann, W. *Chem. Phys. Chem.* **2012**, *13*, 3035−3060. (d) Sun, J.; Liu, C.; Yang, P. *J. Am. Chem. Soc.* **2011**, *133*, 19306−19309. (e) Boettcher, S. W.; Warren, E. L.; Putnam, M. C.; Santori, E. A.; Turner-Evans, D.; Kelzenberg, M. D.; Walter, M. G.; McKone, J. R.; Brunschwig, B. S.; Atwater, H. A.; et al. *J. Am. Chem. Soc.* **2011**, *133*, 1216−1219. (f) Hou, Y.; Abrams, B. L.; Vesborg, P. C. K.; Björketun, M. E.; Herbst, K.; Bech, L.; Setti, A. M.; Damsgaard, C. D.; Pedersen, T.; Hansen, O.; et al. *Nat. Mater.* **2011**, *10*, 434−438. (g) Kumar, B.; Smieja, J. M.; Kubiak, C. P. *J. Phys. Chem. C* **2010**, *114*, 14220−14223. (h) Barton, E. E.; Rampulla, D. M.; Bocarsly, A. B. *J. Am. Chem. Soc.* **2008**, *130*, 6342−6344. (i) Grätzel, M. *Nature* **2001**, *414*, 338−344.

(7) (a) Veldkamp, B. S.; Han, W.-S.; Dyar, S. M.; Eaton, S. W.; Ratner, M. A.; Wasielewski, M. R. *Energy Environ. Sci.* **2013**, *6*, 1917−1928. (b) Andreiadis, E. S.; Jacques, P.-A.; Tran, P. D.; Leyris, A.; Chavarot-Kerlidou1, M.; Jousselme, B.; Matheron, M.; Pécaut, J.; Palacin, S.; Fontecave, M.; Artero, V. *Nat. Chem.* **2013**, *5*, 48−53. (c) Muresan, N. M.; Willkomm, J.; Mersch, D.; Vaynzof, Y.; Reisner, E. *Angew. Chem.* **2012**, *124*, 12921−12925. (d) Valdez, C. N.; Dempsey, J. L.; Brunschwig, B. S.; Gray, H. B. *Proc. Natl. Acad. Sci. U.S.A.* **2012**, *109*, 15589−15593. (e) Marinescu, S. C.; Winkler, J. R.; Gray, H. B. *Proc. Natl. Acad. Sci. U.S.A.* **2012**, *109*, 15127−15131. (f) Li, L.; Duan, L.; Wen, F.; Li, C.; Wang, M.; Hagfeldt, A.; Sun, L. *Chem. Commun.* **2012**, *48*, 988−990. (g) McCrory, C. C. L.; Uyeda, C.; Peters, J. C. *J. Am. Chem. Soc.* **2012**, *134*, 3164−3170. (h) Lakadamyali, F.; Reynal, A.; Kato, M.; Durrant, J.; Reisner, E. *Chem.—Eur. J.* **2012**, *18*, 15464−15475. (i) Solis, B. H.; Hammes-Schiffer, S. *J. Am. Chem. Soc.* **2011**, *133*, 19036−19039. (j) Solis, B. H.; Hammes-Schiffer, S. *J. Inorg. Chem.* **2011**, *50*, 11252−11262. (k) Muckerman, J. T.; Fujita, E. *Chem. Commun.* **2011**, *47*, 12456−12458. (l) Wen, F.; Yang, J.; Zong, X.; Ma, B.; Wang, D.; Li, C. *J. Catal.* **2011**, *281*, 318−324. (m) Zhang, P.; Wang, M.; Li, C.; Li, X.; Dong, J.; Sun, L. *Chem. Commun.* **2010**, *46*, 8806−8808. (n) Dempsey, J. L.; Brunschwig, B. S.; Winkler, J. R.; Gray, H. B. *Acc. Chem. Res.* **2009**, *42*, 1995−2004. (o) Du, P.; Knowles, K.; Eisenberg, R. *J. Am. Chem. Soc.* **2008**, *130*, 12576−12577. (p) Baffert, C.; Artero, V.; Fontecave, M. *Inorg. Chem.* **2007**, *46*, 1817−1824. (q) Hu, X. L.; Cossairt, B. M.; Brunschwig, B. S.; Lewis, N. S.; Peters, J. C. *Chem. Commun.* **2005**, 4723−4725. (r) Razavet, M.; Artero, V.; Fontecave, M. *Inorg. Chem.* **2005**, *44*, 4786−4795. (s) Hu, X.; Brunschwig, B. S.; Peters, J. C. *J. Am. Chem. Soc.* **2007**, *129*, 8988−8998. (t) Connolly, P.; Espenson, J. H. *Inorg. Chem.* **1986**, *25*, 2684−2688. (u) Hawecker, J.; Lehn, J. M.; Ziessel, R. *Nouv. J. Chim.* **1983**, *7*, 271−277.

(8) dmgH = dimethylglyoximate monoanion; $dmgH_2$ = dimethylglyoxime; py = pyridine.

(9) (a) Trogler, W. C.; Stewart, R. C.; Epps, L. A.; Marzilli, L. G. *Inorg. Chem.* **1974**, *13*, 1564−1570. (b) Costa, G.; Tauzher, G.; Puxeddu, A. *Inorg. Chim. Acta* **1969**, *3*, 45−48.

(10) (a) Chen, T.; Amin, I.; Jordan, R. *Chem. Soc. Rev.* **2012**, *41*, 3280−3296. (b) Harnish, B.; Robinson, J. T.; Pei, Z.; Ramström, O.; Yan, M. *Chem. Mater.* **2005**, *17*, 4092−4096. (c) Yan, M.; Harnish, B. *Adv. Mater.* **2003**, *15*, 244−248.

(11) (a) Ciamician, G. *Science* **1912**, *36*, 385−394. (b) Wrighton, M. S. *Science* **1986**, *231*, 32−37. (c) Bard, A. J.; Fox, M. A. *Acc. Chem. Res.* **1995**, *28*, 141−145.

(12) (a) Steenackers, M.; Kueller, A.; Stoycheva, S.; Grunze, M.; Jordan, R. *Langmuir* **2009**, *25*, 2225−2231. (b) Stachowiak, T. B.; Svec, F.; Frechet, J. M. J. *Chem. Mater.* **2006**, *25*, 5950−5957. (c) Wang, H.; Brown, H. R. *Macromol. Rapid Commun.* **2004**, *25*, 1095−1099. (d) Deng, J.-P.; Yang, W.-T.; Ranby, B. *Macromol. Rapid Commun.* **2001**, *22*, 535−538. (e) Milner, S. T. *Science* **1991**, *251*, 905−914.

(13) (a) Seifert, M.; Koch, A. H. R.; Deubel, F.; Simmet, T.; Hess, L. A.; Stutzmann, M.; Jordan, R.; Garrido, J. A.; Sharp, I. D. *Chem. Mater.* **2013**, *25*, 466−470. (b) Steenackers, M.; Gigler, A. M.; Zhang, N.; Seifert, M.; Hess, L. H.; Xuan Lim, C. H. Y.; Loh, K. P.; Garrido, J. A.; Jordan, R.; et al. *J. Am. Chem. Soc.* **2011**, *133*, 10490−10498. (c) Steenackers, M.; Sharp, I. D.; Larsson, K.; Hutter, N. A.; Stutzmann, M.; Jordan, R. *Chem. Mater.* **2010**, *22*, 272−278. (d) Steenackers, M.; Lud, S. Q.; Niedermeier, M.; Bruno, P.; Gruen, D. M.; Feulner, P.; Stutzmann, M.; Garrido, J. A.; Jordan, R. *J. Am. Chem. Soc.* **2007**, *129*, 15655−1566.

(14) Panov, V. P.; Kazarin, L. A.; Dubrovin, V. I.; Gusev, V. V.; Kirsh, Y. E. *Zh. Prikl. Spektrosk.* **1974**, *21*, 862−869.

(15) Chuang, T. J.; Brundle, C. R.; Rice, D. W. *Surf. Sci.* **1976**, *59*, 413−419.

(16) (a) Artero, V.; Fontecave, M. *Chem. Soc. Rev.* **2013**, *42*, 2338−2356. (b) Crabtree, R. H. *Chem. Rev.* **2012**, *112*, 1536−1554. (c) Ostwald, W. *Nature* **1902**, *65*, 522−525.

(17) Surface immobilized catalysts, including those composed of molecular components, are inherently heterogeneized.
(18) (a) Benson, E. E.; Kubiak, C. P.; Sathrum, A. J; Smieja, J. M. *Chem. Soc. Rev.* **2009**, *38*, 89−99. (b) Huff, C. A.; Sanford, M. S. *J. Am. Chem. Soc.* **2011**, *133*, 18122−18125.